Tomographic Imaging Stress Changes in Soil Media

J. C. SANTAMARINA, J. GRAHAM, C. MACDOUGALL, AND V. ROY

The stiffness of particulate media and the velocity of wave propagation are determined by the state of stress. Therefore, boundary measurements of travel time can be inverted to determine the field of velocity and converted to image the state of stress. Results from a simulation study are presented for the cases of footings and tunnels. The underlying assumptions in the simulation are highlighted and difficulties in field implementations are discussed.

The mechanical behavior of soils is determined by the state of stress. The relationship between strength and state of stress is represented in failure criteria such as Mohr-Coulomb. On the other hand, the analysis of particulate arrangements clearly shows the effect of the stress field on deformation parameters (Hertz theory).

It is difficult to measure the state of stress in particulate media. Current technology is based on local measurements with transducers. The presence of the transducer and its relative stiffness affect the measurement. The combined use of stress waves and tomographic inversion to image the field of stress in a medium is discussed. In this case, sources and receivers are mounted on the boundary of the region, with minimum perturbation, and an image of the distribution of the wave velocity is generated by means of mathematical inversion. Finally, velocity (V) is interpreted in terms of stress (σ) by appropriate "constitutive" equations ($\sigma \Leftrightarrow V$).

TOMOGRAPHY

Tomography is an imaging technique based on multiple transmission measurements of time or attenuation. Tomographic reconstruction is the inversion of these spatially averaged boundary measurements, either travel time or amplitude, to determine the field of material parameters in an "unknown space" [see Figure 1 (*a*)].

A possible approach is to discretize the region into pixels [see Figure 1 (*b*)]. Measured travel times are expressed in terms of pixel velocities and travel lengths estimated from assumed ray paths. Assuming a straight ray, the ray path is obtained by joining the source S_a and the receiver R_a; the distance traveled by the ray in pixels 1 and 2 is readily determined (d_{a1} and d_{a2}), and the travel time t_a can be expressed as

$$t_a = \frac{d_{a1}}{V_1} + \frac{d_{a2}}{V_2} \tag{1}$$

where the unknowns are V_1 and V_2. The inverse of the velocity is often referred to as the "slowness" (s). The following equations are written for all the measured travel times [see Figure 1 (*c*)]:

$$\begin{aligned} t_a &= d_{a1} \cdot s_1 + d_{a2} \cdot s_2 \\ t_b &= d_{b3} \cdot s_3 + d_{b4} \cdot s_4 \\ t_c &= d_{c1} \cdot s_1 + d_{c3} \cdot s_3 \\ t_d &= d_{d2} \cdot s_2 + d_{d4} \cdot s_4 \end{aligned} \tag{2}$$

In general, these equations can be written as

$$t_i = \sum_j d_{ij} s_j \tag{3}$$

and the system of Equations 2 can be presented in matrix form,

$$T = D \cdot S \tag{4}$$

where

T = vector of n measured travel times,
D = $n \times m$ matrix of estimated travel lengths, and
S = vector of m unknown pixel slowness.

The goal of inversion is to solve Equation 4 to determine S; then the image is rendered by coloring pixels. For example, gray levels are selected according to the pixels' slowness.

The system of Equation 3 is easily solved for the four unknown values of slowness. In finer grids, normal rays are insufficient; for example, there are six source locations (a–g) yet nine unknown values of pixel slowness in Figure 1 (*d*). Furthermore, not all faces of the unknown region are accessible. In practice, a wave from a source is detected by multiple receivers [see Figure 1 (*e*)]. The result is a system of equations where the number of measured travel times exceeds the number of pixels ($n > m$).

The goal of tomographic reconstruction is to find the best estimate of S. Iterative methods are used to solve the inversion problem and overcome difficulties related to the nature of the problem (e.g., large, sparse, ill-conditioned matrices). Other

J. C. Santamarina, J. Graham, and C. MacDougall, Department of Civil Engineering, University of Waterloo, Ontario N2L 3G1, Canada, V. Roy, Department of Geological Engineering, University of Waterloo, Ontario N2L 3G1, Canada.

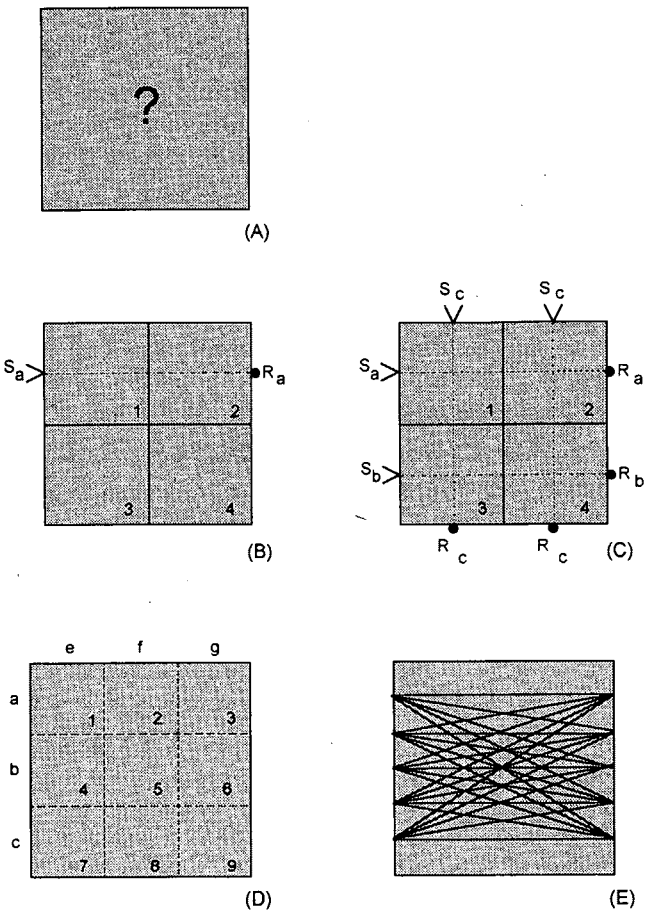

FIGURE 1 Tomographic inversion: (*a*) unknown space; (*b*) discretization into pixels; (*c*) measurement of travel times; (*d*) solution for unknown values of slowness; (*e*) detection by multiple receivers.

solutions include Snell's relations for reflection and refraction, full time series (Fourier slice theorem), and fuzzy logic (norm minimization).

SIMULATION STUDY: PROCEDURE AND ASSUMPTIONS

Step 1: Computation of In Situ and Induced Stresses

The cross section under study is discretized in pixels. At the center of each pixel, the in situ state of stress is computed assuming at-rest conditions, whereas induced stresses are approximated using linear elastic solutions.

Step 2: Computation of Pixel Velocities

Once the state of stress is known, the velocity of wave propagation in the pixel is estimated with constitutive equations that relate stress and velocity ($\sigma \Leftrightarrow V$). Multiple correlations have been proposed between the effective mean confining stress σ'_{mean} and the maximum shear modules G_{max}, shear-wave velocity V_s and compressional wave velocity V_p. However, laboratory experiments in the 1970s and 1980s and simulations with micromechanics have shown that the propagation of P-waves depends primarily on the stress along the direction of propagation (σ_{par}) and that the propagation of S-waves is conditioned by the stresses on the polarization plane (*1*):

$$V_p = \kappa_p \cdot \sigma^{\alpha}_{par} \tag{5}$$

$$V_s = \kappa_s \cdot \sigma^{\beta}_{par} \cdot \sigma^{x}_{nor-1} \cdot \sigma^{\delta}_{nor-2} \tag{6}$$

The constants in these constitutive equations are readily determined in the laboratory. In the case of this study, a true triaxial device was used: a piezocrystal source and sensors were buried in the sample during soil placement, and wave velocities were determined at different states of the stress history. For the purpose of this study, it was assumed that the velocity of propagation V (m/sec) was proportional to the mean stress σ_{mean} (kN/m^2) such that

$$V = 50 + 90 \cdot \sigma^{0.25}_{mean} \tag{7}$$

This corresponds to a nonuniform, vertically heterogeneous isotropic medium, where the velocity increases with depth. A nominal surface velocity of 50 m/sec was used to reduce numerical difficulties related to shallow measurements. In practice, most field cases involve a minimum overburden. (Long and shallow rays should be avoided because of biases induced by excessive ray curvature.)

The exponent $\alpha = 0.25$ corresponded to angular, crushed quartzitic sand. Lower values of α were found in uniform sands with round grains. The higher the α-coefficient, the more significant the effect of stress changes on velocity changes and the lower the effect of noise (such as measurement errors) in the solution. In simulation studies without noise, any realistic value of α can be equally resolved.

Step 3: Computation of Travel Times

Travel times were measured in situ. A digital storage oscilloscope (triggered by a transducer mounted at the source) recorded the source and receiver signals. The relative position of the traces was used to determine travel time. In this study, configurations of sources and receivers simulated real field conditions. Travel times were then integrated along straight rays joining each source and receiver position (Equation 2).

Step 4: Tomographic Inversion

Standard tomographic images were reconstructed using the ART algorithm (*2*). The variation or δ-image was then obtained by subtracting inverted pixel velocities from two consecutive images. In this case, the images obtained were with in situ and combined stresses. The normalized stress change $\Delta\sigma/\sigma_0$ can be obtained from the normalized variation image $\Delta V/V_0$ as

$$\frac{\Delta\sigma}{\sigma_0} = \sqrt[\alpha]{1 + \frac{\Delta V}{V_0}} - 1 \tag{8}$$

SIMULATION CASE STUDIES

Case 1: Strip Footing

The footing was loaded on a semiinfinite medium, characterized by an anisotropic, vertically heterogeneous initial state of stress. Induced stresses were computed using Boussinesq's solution integrated for strip footings. Plane strain was assumed to complete the state of induced stress. The following parameters were used: unit weight of soil $\gamma = 20$ kN/m^3, coefficient of earth pressure at rest $k_0 = 0.4$, Poisson's ratio $\nu = 0.3$, load $q = 100$ kN/m^2, and footing width $B = 2$ m. The imaged cross section was 10 × 10 m. Sources were placed along the right and left sides of the section, and receivers were placed along the left, right, and top sides.

Tomographic reconstruction was based on a 15 × 15 grid. Figure 2 shows (*a*) the image of the in situ state of stress, (*b*) the image of the combined state of stress, and (*c*) the δ-image. Notice the similarity between this image and the stress bulbs predicted by Boussinesq's solution.

Case 2: Multilayer System

A two-layer system loaded with a circular imprint simulates a wheel on a pavement (This problem was first suggested by Stokoe, University of Texas.) In situ stress within the granular layer (Layer 2) was computed using soil $\gamma = 20$ kN/m^3 and an isotropic coefficient $k_0 = 1.0$. Induced stresses were obtained for the two-layer solution (*3*), with $\nu = 0.5$, load $q = 179$ kN/m^2, footing radius $r = 0.3$ m, first-layer thickness $h_1 = 0.3$ m, and relative stiffness $E_1E_2 = 10$.

Tomographic images were limited to the granular base and were generated for the combined state of stress for a 0.6 × 0.6 = m section. Assuming that installation of full instrumentation was possible during construction, travel time data were generated for sources on the left and right sides of the cross section. Sensors were assumed to be installed on left and right sides, between Layers 1 and 2, and within Layer 2 at a depth of 0.6 m.

Simulations with the load (*a*) far from the cross section, (*b*) at the boundary of the cross section, and (*c*) at the center of the cross section were examined (Figure 3). The reconstruction was based on a 12 × 12 grid. In Simulations b and c, the induced stress prevailed over the in situ component, and the field of induced stress became apparent without the need to generate δ-images. The redistribution of stresses within the granular bases by the stiff pavement is clearly shown in the image.

Refracted waves traveling through the faster upper layer were not considered. In field applications, this effect can be minimized by properly selecting the spacing of transducers.

Case 3: Tunnel

For a long circular excavation, stresses were computed by means of Kirsch's solution for an elastic semiinfinite medium and the plane strain condition. The homogenous boundary stresses were estimated assuming that the axis of the tunnel was at a depth of 40 m, soil $\gamma = 20$ kN/m^3, $k_0 = 0.4$, and $\nu = 0.3$. Two tunnels, with diameters of 4 m and 8 m, were modeled. Travel time data were generated simulating the two-borehole tomographic setting with a 20-m spacing. The model assumed 10 sources in one borehole and 10 receivers in the other.

Images were resolved in 10 × 10 pixels, covering the 20- × 20-m region. Images indicated that stresses were low at the crown and the invert of the tunnel but high on the springlines. Although this exercise deviates from reality (e.g., neither support nor plastic regions are involved), the difficulties encountered in this case hint that even greater difficulties will be encountered in real field conditions.

DIFFICULTIES IN FIELD IMPLEMENTATION

Information Content

The images presented previously were generated using different amounts and distributions of information content. The best field setting corresponds to the circular footing on the two-layer medium, where the large number of sources and receivers placed around the cross section led to a high and well-distributed information content. The worst case is the cross-hole configuration used in the tunnels, where most of

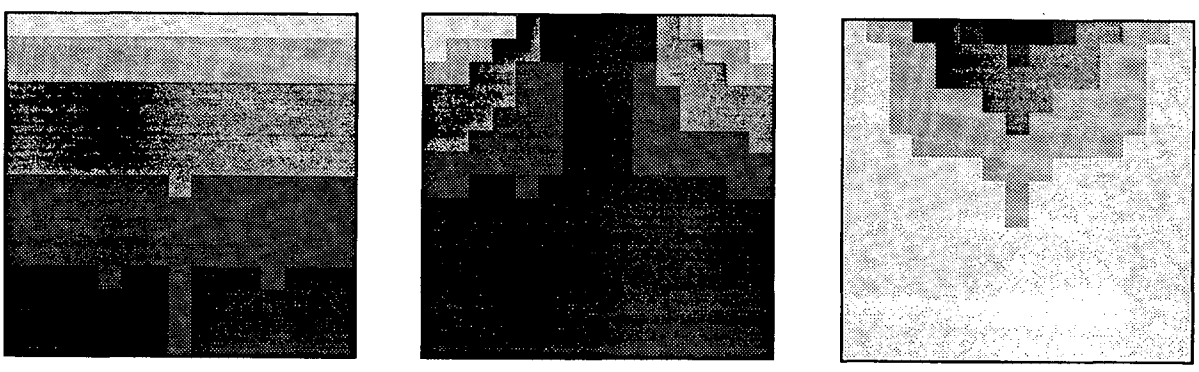

FIGURE 2 Strip load on semiinfinite medium: (*a*) in situ conditions; (*b*) in situ and induced stresses; (*c*) variation image.

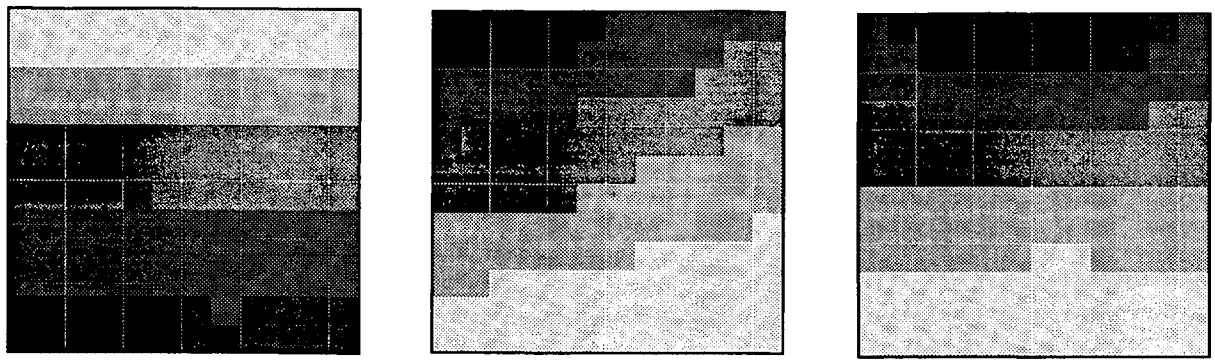

FIGURE 3 Wheel load on two layers (lower layer): (*a*) in situ conditions; (*b*) wheel at the corner; (*c*) wheel at the center.

the limited information is concentrated in the center of the image.

Anisotropy and Vertical Heterogeneity

Wave velocities are related to the stress in the direction of propagation. The state of stress in granular media is heterogeneous and anisotropic; hence the velocity of wave propagation in soil is nonhomogeneous and nonisotropic. Recently, Santamarina and Cesare (*4*) developed a computer program to determine ray paths in anisotropic, vertically heterogeneous media. Figure 4 presents the rays that minimize P-wave travel time in a common geotechnical particulate medium described by the following relationships:

$$V_z^P = 150 \cdot \sigma_z^{0.25} \text{ (vertical heterogeneity)} \quad (9)$$

$$V_x^P = 0.8 \cdot V_z^P \text{ (local anisotropy)} \quad (10)$$

where

V (m/sec) = velocity of propagation in the principal directions x and z,
σ_z (kN/m^2) = vertical effective stress, and
V_x/V_z = 0.8 is an index of anisotropy (often between 0.8 and 1.2).

From an inversion point of view, the deviations from straight rays with changes in depth and inclination (Figure 4), restrict the use of the straight ray assumption.

Diffraction

When the wavelength is in the order of magnitude of the inclusion size, then ray assumptions lose validity, and diffraction must be taken into consideration. In particular, if the inclusion has a lower velocity than the medium, Weilandt (*5*) showed that it may not be detected by inversion algorithms based on travel time. Hence, it follows that imaging a tunnel would be difficult not only from the point of view of angular coverage, which was discussed earlier, but also from the effects of diffraction.

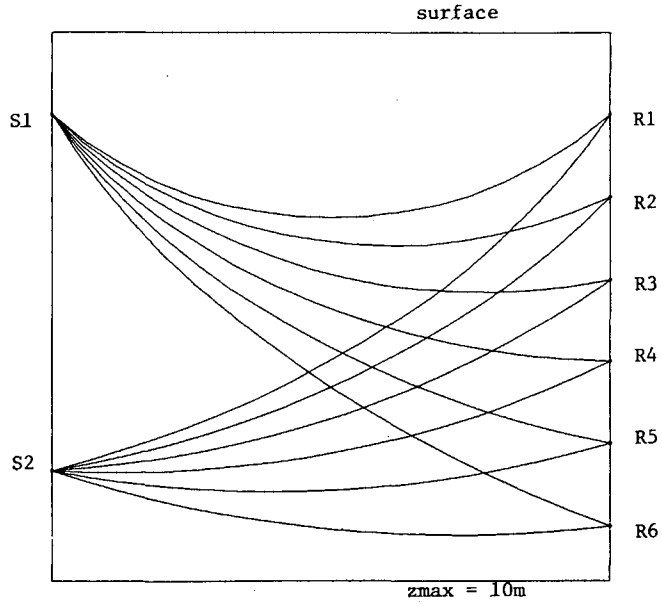

FIGURE 4 Ray paths—anisotropy and vertical heterogeneity.

Field Equipment

Proper selection of adequate sources, receivers, preamplifiers, filters, and digitizers is most important to successfully implementing the proposed technology.

CONCLUSIONS

It is possible to image the state of stress in granular media. Results are enhanced when variation images are produced. An alternative to "variation images" is the "imaging of variations" where changes in measured travel times are inverted (not shown here).

Preliminary results indicate that inverting changes is a more robust approach in cases where the medium is not weakly heterogeneous.

The simple cross-hole tomographic setting is inherently difficult to resolve (such as in the case of deep tunnels).

Small stress changes or stress changes that result in a region of velocity lower than the medium may not be properly detected, particularly if long wavelengths are used and diffraction takes place.

The anisotropy and heterogeneity induced by the in situ state of stress and by the stress changes affect the characteristics of wave propagation, further complicating the inversion problem.

ACKNOWLEDGMENTS

This study was part of a research program on wave-geomedia interaction and applications. Support was provided by the National Science Foundation and the Natural Sciences and Engineering Research Council of Canada.

REFERENCES

1. Knox, D. P., K. H. Stokoe, and S. E. Kopperman. *Effect of State of Stress on Velocity of Low-Amplitude Shear Waves Propagating Along Principal Stress Directions in Dry Sand.* Report GR82-83. University of Texas at Austin, 1982.
2. Tallin, A. G., and J. C. Santamarina. Geotomography in Site Investigations: Simulation Study. *Geotechnical Testing Journal*, Vol. 13, No. 2, 1990, pp. 129–133.
3. Poulos, H. G., and E. G. Davis. *Elastic Solutions for Soil and Rock Mechanics*. John Wiley and Sons, Inc., New York, 1974.
4. Santamarina, J. C., and M. A. Cesare. *Inversion Problems in Anisotropic, Vertically Heterogeneous Media*. Department of Civil Engineering, University of Waterloo, Waterloo, Ontario, Canada, 1992.
5. E. Wielandt. On the Validity of Ray Approximation for Interpreting Delay Times. In *Seismic Tomography* (G. Nolet, ed.), Reidel Publishing Company, Boston, 1987, pp. 85–98.

Publication of this paper sponsored by Committee on Soil and Rock Properties.